

**ZINC OXIDE NANOSTRUCTURES GROWN
USING ELECTRIC FIELD-ASSISTED AQUEOUS
SOLUTION METHOD FOR UV
PHOTODETECTOR APPLICATIONS**

by

RAMAZANALI DALVAND

**Thesis submitted in fulfillment of the requirements
for the degree of
Doctor of Philosophy**

June 2019

DEDICATION

TO

MY WIFE AND MY CHILDREN

ACKNOWLEDGEMENT

First and foremost, I would like to thank Allah for granting me good health and patience to complete this research. I would also like to express sincere gratitude to my main supervisor, Associate Professor Dr. Shahrom Bin Mahmud for his intellectual guidance; devoted time and support in completing this study, who helped me through difficult times in my research work. I would like to express my appreciation to my co-supervisor, Associate Professor Dr. Azman Bin Pkm Seeni Mohamed for his guidance throughout my study. I express my gratitude as well to all staff members of the School of Physics, USM for their encouragement. I also express appreciation to the staff of the Institute of Nano-Optoelectronics Research and Technology (INOR) for their technical assistance during my laboratory work, particularly in the sample characterizations. I would like to thank my wife for her endless support, sympathy and encouragement during the period of the study. Finally, my deepest and heartfelt gratitude goes to my children for their patience while I took time away from them for my studies and writing this thesis.

TABLE OF CONTENTS

| | |
|--|------|
| ACKNOWLEDGEMENT | ii |
| TABLE OF CONTENTS | iii |
| LIST OF TABLES | viii |
| LIST OF FIGURES | ix |
| LIST OF ABBREVIATIONS | xiii |
| LIST OF SYMBOLS | xvi |
| ABSTRAK | xix |
| ABSTRACT | xxi |
| | |
| CHAPTER 1 - INTRODUCTION | |
| 1.1 Introduction | 1 |
| 1.2 Research problem and motivation | 2 |
| 1.3 Scope of study | 4 |
| 1.4 Objectives of thesis | 4 |
| 1.5 Originality of the Research Works | 5 |
| 1.6 Outline of the thesis | 5 |
| | |
| CHAPTER 2 - THEORETICAL BACKGROUND AND LITERATURE | |
| REVIEW | |
| 2.1 Introduction | 7 |
| 2.2 Nanomaterials | 7 |
| 2.3 Overview of ZnO and ZnO nanostructures | 9 |
| 2.3.1 Lattice parameters and crystal structures of ZnO | 10 |

| | | |
|-------|---|----|
| 2.3.2 | Optical properties of ZnO | 13 |
| 2.4 | Overview of substrate | 15 |
| 2.4.1 | Porous silicon (PSi) substrate | 16 |
| 2.5 | Overview of electric field-assisted aqueous solution technique | 18 |
| 2.5.1 | The electric field-assisted aqueous solution technique | 18 |
| 2.5.2 | Mechanism of electric field-assisted aqueous solution technique | 21 |
| 2.5.3 | Numerous advantages of use the electric field-assisted aqueous solution technique | 22 |
| 2.6 | Overview of one-dimensional ZnO nanorod-like arrays growth conditions | 22 |
| 2.6.1 | Mechanism of one-dimensional ZnO nanorod-like arrays growth conditions | 22 |
| 2.6.2 | Literature review of one-dimensional ZnO nanorod-like arrays | 24 |
| 2.7 | Ultraviolet photodetection | 26 |
| 2.7.1 | Literature review on 1-D ZnO UV photodetection | 27 |
| 2.7.2 | Theoretical concepts of ultraviolet detection | 28 |
| | 2.7.2(a) Photoconductivity | 30 |
| | 2.7.2(b) The photoconduction mechanism in 1-D ZnO nanostructures | 33 |

CHAPTER 3 - EXPERIMENTAL EQUIPMENT AND METHODOLOGY

| | | |
|-------|---|----|
| 3.1 | Experimental Equipment | 36 |
| 3.1.1 | Introduction | 36 |
| 3.1.2 | Photo electrochemical etching Teflon cell | 36 |
| 3.1.3 | Electric field-assisted aqueous solution (EFAS) Teflon cell | 37 |
| 3.1.4 | Direct current (DC)/ Radio frequency (RF)-sputtering system | 38 |

| | | |
|----------|--|----|
| 3.1.5 | Thermal annealing processes | 39 |
| 3.1.6 | Structural and morphological tools | 40 |
| 3.1.6(a) | X -ray diffraction | 41 |
| 3.1.6(b) | Field emission scanning electron microscopy | 43 |
| 3.1.6(c) | Energy Dispersive X-ray analysis | 46 |
| 3.1.6(d) | Atomic force microscopy | 47 |
| 3.1.6(e) | Transmission electron microscopy | 49 |
| 3.1.7 | Instruments utilized to optical characterization of the ZnO nanostructures | 51 |
| 3.1.7(a) | Photoluminescence spectroscopy | 51 |
| 3.1.7(b) | Raman spectroscopy | 53 |
| 3.1.7(c) | Ultraviolet-visible spectroscopy | 56 |
| 3.1.7(d) | Optical reflectometer | 58 |
| 3.1.8 | Current-time and current-voltage measurements system | 59 |
| 3.2 | Methodology | 60 |
| 3.2.1 | Introduction | 60 |
| 3.2.2 | Preparation and cleaning of porous silicon substrate | 63 |
| 3.2.3 | Deposition of the ZnO seed-layer on the prepared substrates | 64 |
| 3.2.4 | Annealing process of the ZnO seed-layer | 65 |
| 3.2.5 | Synthesis of the ZnO nanostructures using the electric field-assisted aqueous solution technique | 65 |
| 3.2.6 | Characterization of structural and optical of the samples | 67 |
| 3.2.7 | The ultraviolet photodetector fabrication and characterization | 68 |

CHAPTER 4 - GROWTH OF 1-D ZnO NANOSTRUCTURE ARRAYS

| | | |
|-------|---|----|
| 4.1 | Growth and characterization of the 1-D ZnO nanostructure arrays on porous silicon substrates with different current densities | 70 |
| 4.1.1 | Introduction | 70 |
| 4.1.2 | Observation of porous silicon | 70 |
| 4.1.3 | Surface morphology by FESEM microscopy | 71 |
| 4.1.4 | X-ray diffraction analysis | 76 |
| 4.1.5 | Photoluminescence measurements | 79 |
| 4.1.6 | Raman spectra | 83 |
| 4.2 | Growth and characterization of ZnO nanostructures on porous silicon substrate with different precursor concentrations | 86 |
| 4.2.1 | Introduction | 86 |
| 4.2.2 | Observation of porous silicon | 86 |
| 4.2.3 | Surface morphology using Field emission scanning electron microscopy | 87 |
| 4.2.4 | X-ray diffraction analysis | 91 |
| 4.2.5 | Photoluminescence measurements | 93 |
| 4.2.6 | Raman spectra | 96 |
| 4.3 | Summary | 97 |

CHAPTER 5 - ULTRAVIOLET PHOTODETECTOR

| | | |
|-------|---|-----|
| 5.1 | Introduction | 99 |
| 5.2 | Ultraviolet photodetector based on well-aligned ZnO nanoneedle arrays grown on porous silicon substrate | 99 |
| 5.2.1 | Characterization of needle-shaped ZnO nanostructures grown on porous silicon substrate | 99 |
| 5.2.2 | Ultraviolet photodetection by ZnO nanoneedle arrays on porous silicon substrate | 103 |

| | | |
|---|---|-----|
| 5.3 | Ultraviolet photodetector based on well-aligned ZnO nanocone arrays grown on porous silicon substrate | 110 |
| 5.3.1 | Characterization of cone-shaped ZnO nanostructure arrays grown on porous silicon substrate | 110 |
| 5.3.2 | Ultraviolet photodetection by ZnO nanocone arrays on porous silicon substrate | 110 |
| 5.4 | Summary | 115 |
| CHAPTER 6 - CONCLUSIONS AND FUTURE WORKS | | |
| 6.1 | Conclusions | 117 |
| 6.2 | Future work | 118 |
| REFERENCES | | 120 |

LIST OF PUBLICATIONS

LIST OF TABLES

| | | Page |
|-----------|--|-------------|
| Table 2.1 | Summary of 1-D ZnO UV photodetectors with their response and recovery times, substrate, structural used, light-detection wavelength, and applied bias voltage. | 29 |
| Table 3.1 | The magnetron RF sputtering conditions for the ZnO seed layers on PSi substrates. | 65 |
| Table 4.1 | Details of XRD patterns of ZnO nanostructures with different current densities. | 79 |
| Table 4.2 | Summarized data from the PL spectra of 1-D ZnO nanostructures. | 83 |
| Table 4.3 | Details of XRD patterns of ZnO nanostructures with various precursor concentrations. | 93 |
| Table 4.4 | Summarized data from the PL spectra of ZnO nanostructures with various precursor concentrations. | 95 |
| Table 5.1 | Electrical properties of ZnO nanoneedles-based UV photodetectors at different applied bias voltages. | 106 |
| Table 5.2 | The comparison between the literature and the current study of the photoelectrical parameters of ZnO-Based UV photodetectors. | 108 |
| Table 5.3 | Electrical properties of ZnO nanocones-based UV photodetectors at different applied bias voltages. | 112 |

LIST OF FIGURES

| | | Page |
|------------|--|-------------|
| Figure 2.1 | (a) The rock-salt and (b) zinc-blende structures of ZnO. | 11 |
| Figure 2.2 | (a) The hexagonal wurtzite structure and (b) hexagonal unit cell of ZnO. | 12 |
| Figure 2.3 | (a) Miller indices of several lattice planes in a hexagonal lattice of ZnO and (b) hexagonal unit cell and indices of several lattice directions. | 13 |
| Figure 2.4 | Schematic diagram of the typical photoconductor with an applied external bias-voltage V. | 30 |
| Figure 2.5 | Schematic diagrams of the photoconduction mechanism in a ZnO nanowire: (a) schematic illustration of the ZnO nanowire photodetector, (b) the oxygen-trapping mechanism in ZnO nanowire in the dark condition, (c) the hole-trapping and photoconduction process in ZnO nanowire under UV-illumination. | 35 |
| Figure 3.1 | Schematic of the photo electrochemical etching Teflon cell used to fabricate porous silicon. | 37 |
| Figure 3.2 | Schematic of the screw-capped Teflon cell used to synthesis one-dimensional ZnO nanostructures. | 38 |
| Figure 3.3 | A schematic diagram of (a) the DC/RF sputtering chamber and (b) Edwards (A500) DC/RF magnetron sputtering system. | 39 |
| Figure 3.4 | A schematic diagram of (a) a thermal annealing furnace and (b) LENTON VTF/12/60/700 thermal annealing furnace system. | 40 |
| Figure 3.5 | Several of information that can be obtained from XRD pattern. | 42 |
| Figure 3.6 | A schematic diagram of (a) Experimental set-up of the HR-XRD system and (b) Image of the HR-XRD system model (PANalytical X'Pert PRO MRD PW3040). | 43 |
| Figure 3.7 | A schematic diagram of (a) FESEM configuration and (b) Image of the FESEM system model (FESEM-FEI/Nova NanoSEM 450). | 46 |

| | | |
|-------------|---|----|
| Figure 3.8 | A schematic diagram of atomic force microscopy configuration. | 48 |
| Figure 3.9 | Photograph of the atomic force microscopy system. | 48 |
| Figure 3.10 | A schematic of typical TEM system. | 50 |
| Figure 3.11 | Schematic diagram of electron optics of a TEM system in imaging (a) and diffraction (b) modes. | 50 |
| Figure 3.12 | PL instrument set-up configuration. | 52 |
| Figure 3.13 | The E_a , E_d and E_i reveal the energy level of acceptor, donor and intermediate, respectively. (a-d) show the radiative recombination processes and (e) shows the non-radiative recombination, respectively. | 53 |
| Figure 3.14 | (a) Schematic diagrams of the Rayleigh scattering, Raman stokes and Raman anti-stokes scattering processes. The ν_i and ν_f are initial and final states, respectively. (b) The Image of Raman and photoluminescence spectroscopy system. | 55 |
| Figure 3.15 | Schematic diagram of UV-Visible spectroscopy. | 57 |
| Figure 3.16 | Typical UV-Visible transmission spectrum; the bandgap energy of the sample is determined from the intersection of linear interpolation of spectrum and x-axis. | 58 |
| Figure 3.17 | Image of Optical reflectometry (Filmetrics F20) system. | 59 |
| Figure 3.18 | Experiment flow chart | 61 |
| Figure 3.19 | Flow chart of the methodology and fabrication processes. | 62 |
| Figure 3.20 | Schematic of the screw-capped Teflon cell used to synthesis one-dimensional ZnO nanostructures. | 67 |
| Figure 3.21 | Schematic diagram of the metal Pt contacts for ZnO MSM Photodetector (a); Top view image of the ZnO nanoneedles MSM photodetector (b). | 69 |
| Figure 3.22 | Schematic diagram of the experimental set-up for UV photoresponse measurement. | 69 |
| Figure 4.1 | (a) The FESEM image of pure PSi substrate, (b) 3-dimensional view of the AFM image of ZnO/PSi substrate, and (c) The AFM image of ZnO/Si substrate. | 71 |
| Figure 4.2 | Cross-sectional, top and higher-magnification FESEM images of the ZnO nanostructures grown at (a) 0.0 mA (b) 0.05 mA (c) 0.1mA (d) 0.5 mA (e) 0.75 mA. | 73 |

| | | |
|-------------|--|-----|
| Figure 4.3 | XRD patterns of ZnO nanostructures grown at different current densities. | 77 |
| Figure 4.4 | PL spectra of the bare PS substrate. | 81 |
| Figure 4.5 | PL spectra patterns of ZnO nanostructures grown at different current densities. | 82 |
| Figure 4.6 | Raman spectra of the ZnO nanostructures grown at different current densities. | 85 |
| Figure 4.7 | (a) FESEM image of pure PSi substrate, and (b) 3-dimensional view of the AFM image pure PSi substrate. | 87 |
| Figure 4.8 | Cross-sectional, top and higher-magnification FESEM images of the ZnO nanostructures grown at (a) 10 mM (b) 25 mM (c) 50 mM (d) 75 mM. | 90 |
| Figure 4.9 | XRD patterns of ZnO nanostructures grown with various precursor concentrations: (a) 10 mM, (b) 25 mM, (c) 50 mM and (d) 75 mM. | 92 |
| Figure 4.10 | PL spectra patterns of ZnO nanostructures grown on PSi substrates with various precursor concentrations. | 95 |
| Figure 4.11 | Raman spectra of the ZnO nanostructures with various precursor concentrations: (a) 10 mM, (b) 25 mM, (c) 50 mM, and (d) 75 mM. | 97 |
| Figure 5.1 | XRD pattern of ZnO nanoneedle arrays grown on the PSi substrate. | 100 |
| Figure 5.2 | Room temperature PL spectrum of ZnO nanoneedle arrays grown on PSi substrate. | 100 |
| Figure 5.3 | Cross-sectional, higher-magnification and top FESEM images of the ZnO nanoneedles synthesized on the PSi substrate. | 102 |
| Figure 5.4 | EDX spectrum of vertically aligned ZnO nanoneedles synthesized on ZnO/PSi substrate. | 102 |
| Figure 5.5 | (a) TEM image of the ZnO nanoneedles and (b) the SAED pattern from an individual ZnO nanoneedle. | 103 |
| Figure 5.6 | Schematic illustration of the UV photodetector structure. | 104 |
| Figure 5.7 | Current-voltage characteristics of the MSM-structured UV-photodetector measured in dark and under UV-illumination. | 105 |

| | | |
|-------------|--|-----|
| Figure 5.8 | UV-photodetector photoconductivity versus light wavelength. | 106 |
| Figure 5.9 | Photocurrent response under on/off UV-light radiation with the illumination wavelength of 325 nm at various bias voltages. | 109 |
| Figure 5.10 | Current-voltage characteristics of the MSM-structured UV-photodetector measured in dark and under UV-illumination. | 111 |
| Figure 5.11 | Photocurrent response under on/off UV-light radiation with the illumination wavelength of 325 nm at various bias voltages. | 114 |

LIST OF ABBREVIATIONS

| | |
|--------|---|
| a.u. | Arbitrary unit |
| AFM | Atomic force microscopy |
| CCD | Charge coupled device |
| CBD | Chemical bath deposition |
| CRD | Cathode ray display |
| CVD | Chemical vapor deposition |
| CB | Conduction band |
| I-T | Current-Time |
| I-V | Current-Voltage |
| DLE | Deep-level emission |
| DI | Deionized |
| DC | Direct current |
| EFAS | Electric field-assisted aqueous solution |
| EDX | Energy dispersive X-ray |
| EIS | Electrochemical impedance spectroscopy |
| eV | Electron volt |
| FFT | Fast Fourier transform |
| FESEM | Field emission scanning electron microscopy |
| FTO | Fluorine doped tin oxide |
| FWHM | Full width at half maximum |
| FRA | Frequency response analysis |
| HMT | Hexamethylenetetramine |
| HR-XRD | High resolution-X ray diffraction |

| | |
|--------|---|
| HR-TEM | High resolution-transmission electron microscopy |
| IHP | Inner Helmholtz plane |
| ITO | Indium tin oxide |
| LED | Light emitting diode |
| LO | Longitudinal optic |
| E | Light irradiance |
| MOCVD | Metal organic chemical vapor deposition |
| MSM | Metal-semiconductor-metal |
| MBE | Molecular beam epitaxy |
| NBE | Near band emission |
| 1-D | One dimensional |
| OHP | Outer Helmholtz plane |
| PECE | Photo electrochemical etching |
| PL | Photoluminescence |
| PVD | Physical vapor deposition |
| PC | Polycarbonate |
| PEN | Polyethylene naphthalate |
| PES | Polyethersulfone |
| PET | Polyethylene terephthalate |
| PSD | Phase sensitive detection |
| PI | Polyimide |
| PSi | Porous silicon |
| RCA | Radio corporation of America (cleaning procedure) |
| RF | Radio frequency |
| RT | Room temperature |

| | |
|------------|--|
| SAED | Selected area electron diffraction |
| C_{6v}^4 | Schoenflies notation of space group of hexagonal ZnO |
| TEM | Transmission electron microscopy |
| TO | Transverse optic |
| UV | Ultraviolet |
| Vis | Visible |
| XRD | X-ray diffraction |

LIST OF SYMBOLS

| | |
|------------|---------------------------------------|
| A | Area |
| D | Average crystal size |
| R_a | Accumulation resistance |
| q | Charge of electron |
| R_{ct} | Charge transfer resistance |
| Q | Constant phase element |
| σ_0 | Conductivity in dark |
| σ | Conductivity in the presence of light |
| I_0 | Current in dark |
| I | Current in the presence of light |
| J | Current density |
| J_n | Current density of electron |
| J_p | Current density of hole |
| E_C | Conduction band |
| I_{dark} | Dark current |
| R_d | Diffuse layer resistance |
| C_{dl} | Double-layer capacitance |
| E | Electric field |
| n_0 | Electron concentration at equilibrium |
| μ_n | Electron mobility |
| E_g | Energy gap |
| E_a | Energy level of acceptor |

| | |
|-----------|---|
| E_d | Energy level of donor |
| E_i | Energy level of intermediate |
| R_f | Film resistance |
| ν | Frequency of light |
| E_F | Fermi level of semiconductor |
| ν_f | Final state |
| p_0 | Hole concentration at equilibrium |
| μ_p | Hole mobility |
| θ | Incident / Diffraction angle |
| Z_c | Impedance |
| ν_i | Initial state |
| d | Interplanar spacing of the crystal planes |
| a | Lattice constant |
| c | Lattice constant |
| τ_n | Lifetime of carriers |
| (hkl) | Miller indices |
| G_0 | Net optical generation rate |
| P_{opt} | Optical power of the incident light |
| I_{ph} | Photocurrent |
| R_p | Polarization resistance |
| S | Photosensitivity |
| η | Quantum efficiency |
| Z_0 | Resistance before exposed |
| Z_s | Resistance after exposed |

| | |
|--------------------|-------------------------------|
| R_λ | Responsivity of photodetector |
| ε_{zz} | Strain along c-axis |
| t | Time |
| τ_t | Transit time of carriers |
| Δ | Thermal energy |
| V | Voltage |
| Z_w | Warburg impedance |
| λ | Wavelength |
| w | Width |

**STRUKTUR NANO ZINK OKSIDA DITUMBUH MELALUI
KAEDAH LARUTAN AKUEUS BANTUAN-MEDAN ELEKTRIK UNTUK
APLIKASI PENGESANFOTO UV**

ABSTRAK

Struktur nano zink oksida (ZnO) telah berjaya disintesis menggunakan teknik larutan akueus berbantu-medan elektrik (EFAS). Nano struktur nano ZnO telah ditumbuh dengan parameter pertumbuhan berbeza dan dicirikan untuk ciri struktur, optik dan elektrik. Kajian ini menggunakan silikon berliang (PSi) berbenih-ZnO untuk menumbuhkan struktur nano ZnO satu-dimensi (1-D). Tatasusunan nanorod ZnO disintesis melalui pengoptimuman ketumpatan arus menggunakan kaedah EFAS dan nanorod ZnO ditumbuh di atas subtract Psi yang disediakan melalui teknik punaran elektrokimia foto (PECE). Sampel jejaring jalaran menegak ZnO yang disediakan pada ketumpatan arus 0.5 mA/cm², suhu pertumbuhan 105 °C, kepekatan prekursor 50 mM, dan tempoh pertumbuhan 60 minit menghasilkan ciri optimal struktur, morfologi dan optik dengan keamatan puncak XRD tertinggi (002). Tambahan pula, data kefotopendarcahayaan (PL) dan Raman sampel optima menunjukkan nisbah keamatan tertinggi antara pemancaran pinggir-jalur-dekat dan pemancaran aras-mendalam manakala data Raman menunjukkan keamatan tertinggi mod fonon E₂ (tinggi) jika dibandingkan dengan nilai sampel lain. Dengan menggunakan kepekatan prekursor optima dalam kaedah EFAS, struktur nano ZnO 1-D ditumbuh atas sustrat PSi. Nanorod ZnO 1-D dengan kepala kon dihasilkan menggunakan teknik EFAS bilamana parameter penumbuhan ditala pada kepekatan prekursor 50 mM, ketumpatan arus 0.65 mA/cm², suhu penumbuhan 105 °C dan tempoh penumbuhan 60 minit. Nanorod kepala kon tersebut memiliki kualiti kristal yang baik dan mempamerkan puncak UV

yang paling tajam dan paling amat berbanding dengan nilai sampel lain. Dua jenis fotopengesan UV logam-semikonduktor-logam (MSM) telah difabrikasi atas substrat P-Si – pertama diasaskan oleh tatasusunan nanojarum ZnO menegak dari parameter penumbuhan optima manakala yang kedua diasaskan oleh tatasusunan nanorod ZnO kepala kon. Ciri optoelektronik fotopengesan UV yang difabrikasi telah dikaji dalam persekitaran gelap dan dikaji bawah pencahayaan UV 325 nm. Apabila didedahkan kepada cahaya UV pada voltan pincang 3 V, fotopengesan UV berasaskan tatasusunan nanojarum menunjukkan responsiviti yang tinggi pada 1.98 A/W, dan tempoh respon 86 ms dan tempoh pemulihan 83 ms manakala fotopengesan UV berasaskan tatasusunan nanorod ZnO kepala kon mempamerkan tempoh respon 191 ms dan tempoh pemulihan 209 ms. Kebaharuan utama kajian ini melibatkan penumbuhan memilih mudah untuk morfologi kepala nanorod/nanojarum ZnO dengan penalaan ketumpatan arus (kurang dari 1 mA/cm²) dalam kaedah EFAS.

ZINC OXIDE NANOSTRUCTURES GROWN USING ELECTRIC FIELD- ASSISTED AQUEOUS SOLUTION METHOD FOR UV PHOTODETECTOR APPLICATIONS

ABSTRACT

Nanostructured zinc oxide (ZnO) was successfully synthesized using an electric field-assisted aqueous solution (EFAS) technique. ZnO nanostructures were grown with different growth parameters and characterized for the structural, optical and electrical properties. The study employed ZnO-seeded porous silicon (PSi) to grow one-dimensional (1-D) ZnO nanostructures. ZnO nanorod arrays were synthesized via the optimization of current density by using EFAS method and the ZnO nanorods were grown on PSi substrates that were prepared via a photo electrochemical etching (PECE) technique. Vertically aligned needle-shaped ZnO sample prepared at a current density of 0.5 mA/cm^2 , growth temperature of $105 \text{ }^\circ\text{C}$, precursor concentration of 50 mM , and growth duration of 60 minutes produced the optimal structural, morphological, and optical properties with the highest (002) XRD peak intensity. Moreover, photoluminescence (PL) data of the optimized sample revealed the highest near-band-edge emission to deep-level emission intensity ratio while Raman data showed the most intense E2 (high) phonon mode compared with that of other samples. Using the optimized precursor concentration in the EFAS method, 1-D ZnO nanostructure arrays were grown on PSi substrates. 1-D ZnO nanorods with cone heads were produced using the EFAS technique when the growth parameters were tuned at 50 mM precursor concentration, 0.65 mA/cm^2 current density, $105 \text{ }^\circ\text{C}$ growth temperature and 60 minutes growth duration. The cone head nanorods had good crystal quality and exhibited the sharpest and most intense UV peak compared with that of

other samples. Two types of metal–semiconductor-metal (MSM) UV photodetectors were fabricated on PSi substrates – one was based on vertical ZnO nanoneedle array from optimized growth parameters while the second one was based on the cone-head ZnO nanorod arrays. The optoelectronic characteristics of the fabricated UV photodetectors were studied in the dark environment and under 325 nm UV light illumination. Upon exposure to the UV light at 3 V bias voltage, the ZnO nanoneedle arrays UV photodetector showed a high responsivity of 1.98 A/W, fast response of 86 ms and recovery time of 83 ms while the UV photodetector fabricated with cone-head ZnO nanorods exhibited the response and recovery times of 191 ms and 209 ms, respectively. The prime novelty of this work involved the convenient selective growth of tip morphology of ZnO nanorods/nanowires by tuning the current density (less than 1 mA/cm²) of the EFAS method.

CHAPTER 1

INTRODUCTION

1.1 Introduction

Zinc oxide (ZnO) nanostructures have appeared as one of the most versatile oxide materials due to their numerous industrial usages in the as catalysts, pigments, medicine, rubber additives and ceramics additives. ZnO is inherently n-type semiconductor with a wide direct band gap of 3.37 (eV) and a large exciton binding energy of 60 (meV); therefore, it has excellent properties such as good thermal-mechanical stability and unique electronic-optical properties [1].

ZnO is a functional material that exist in different growth morphologies that include nanorod, nanobelt, nanosphere, nanotube, nanowire, nanosheet, nanoring, and flowers-like structure. Amongst various one-dimensional (1-D) semiconductor nanomaterials, ZnO has been the most studied in recent decade because of its fast response, slow electron/hole recombination rate, high surface area-to-volume ratio, high optical gain, and unique crystalline orientation. Production of 1-D ZnO with controlled diameters is important since the ZnO nanostructure can be used in diverse applications such as field-effect transistors [2], nanolasers [3], light emitting diodes [4], photodetectors [5], chemical and biosensors [6, 7], solar cells, next-generation UV sources [8], field-emission devices [9], nanogenerators [10], and photocatalysts, [11]. A number of methods such as spray pyrolysis [12], pulsed laser deposition [13], sol-gel method [14], chemical bath deposition [15], electrochemical deposition [16], metalorganic chemical vapor deposition [17], and hydrothermal [18], have been utilized to fabricate 1-D ZnO nanostructures on different types of substrates.

1.2 Research problem and motivation

The properties of ZnO nanostructures are known to be strongly depended on their size, morphology and tip shape. The performance of their applications such as UV sensitivity is very much dependent on their size, morphology and tip shape whereby a good control during synthesis is needed in order to obtain a homogenous array of ZnO nanostructures with a desired size, morphology and tip. Tuning the morphology, size and tip shape of 1-D nanostructures grown on porous silicon (PSi) substrates has been a challenging effort. In recent years, many studies have been performed to syntheses uniform 1-D ZnO nanostructures on a variety of substrates because of their specific optoelectronic properties, leading to promising applications in the fabrication of functional nano-devices. The design of 1-D ZnO nanostructures in array is of importance for development of optoelectronic applications. Among the numerous research on the synthesis and properties of the ZnO nanostructures, uniform ZnO nanorods have been successfully prepared through the Au catalysed vapor transport-condensation technique and vapor-phase growth with or without using a GaN template [19-21]. However, the presence of Au impurities can be not only detrimental to the intrinsic physical properties of nanorods but also harmful to their applications in nanodevices. Hence, the choice of suitable method is important to achieve and control size, shape and tip shape of the produced nanostructured materials, without using any additives or metal catalysts and template. To date, randomly distributed 1-D ZnO nanostructures have been achieved on the substrates via different methods [22-24], and individual ZnO nanostructures dispersed in solution have been synthesized via sol-gel reaction [25]. However these ZnO nanostructures are not suitable for the fabrication of optoelectronic devices as they were not grown erectly on planar conducting substrates. Although, ZnO vertical nanotapered arrays were

fabricated on Si substrates by thermal evaporation [26], however, there was very limited control over the sharpness of the ZnO-nanotapers that has great effect on the performance of photonic devices. Therefore, to overcome the process control problem, efforts need to be invested to precisely control their size, tip shape, and surface architecture to utilize ZnO for various practical fields. In this work, the electric field-assisted aqueous solution method was used as a good technique to precisely tune the shape and morphology of ZnO nanostructures on PSi substrates.

ZnO nanostructures can be obtained either via vapor-phase or via solution-phase synthetic methods. However, the vapor-phase synthetic methods consume a large amount of energy and require special equipment with rigid experimental conditions [27-30]. Therefore, these limitations inspired the research on the solution-phase synthesis, which offers a great potential for a low cost and large-scale fabrication. The low-temperature solution methods (typically <110 °C) are particularly attractive because of the low-energy requirements and environmentally benign synthetic conditions. However, the low growth temperatures tend to favour excess point defect levels or even a breakdown of crystalline growth into an amorphous one [31]. The electric field-assisted aqueous solution (EFAS) process is similar to electrochemical deposition except that the temperature can be selected higher than 90 °C while the electrochemical deposition is typically conducted at a considerably lower temperature (usually from 60 °C to 90 °C). Accordingly, the process can be called EFAS when the growth temperature is chosen around 100 °C. Therefore, the optical properties of nanostructured materials can be further improved if growth occurs at a high-temperature compared with those synthesized by other solution-phase techniques especially chemical bath deposition and electrochemical deposition. Thus, the EFAS method has potential to the decrease of defect density of deposited nanostructures. The

EFAS method is a new and easy way to grow 1-D ZnO nanostructure arrays. The main advantages of this approach are good controls of chemical composition and morphology, low growth temperature, capability for large-scale production, simplicity, and environmental friendly.

1.3 Scope of study

The scope is focused on bottom-up growth of ZnO nanostructures using EFAS method grown on porous silicon substrates that were used to detect UV light. This study optimized the growth parameters such as current density and precursor concentration to produce 1-D ZnO nanostructure arrays on porous silicon substrate using the EFAS technique. The porous silicon layer was prepared through a photo-electrochemical etching method. The optical and structural properties of the ZnO nanostructures were investigated by Atomic force microscopy (AFM), X -ray diffraction (XRD), Field emission scanning electron microscopy (FESEM), Transmission electron microscopy (TEM), Photoluminescence (PL) spectroscopy and Raman spectroscopy at room temperature. The needle-shaped and cone-shaped ZnO nanostructure arrays were used to fabricate UV photodetectors.

1.4 Objectives of thesis

The main objectives of this thesis are summarized in the following points:

1. To synthesis 1-D ZnO nanostructure arrays on porous silicon substrates using electric field-assisted aqueous solution (EFAS) method.
2. To evaluate the effect of changing the current density and precursor concentration on the structural and optical properties of the aligned ZnO nanostructure arrays synthesized on PSi substrate.

3. To fabricate and evaluate the performance of metal-semiconductor-metal (MSM) UV photodetectors based on the needle-shaped and cone-shaped ZnO nanostructure arrays on PSi substrates.

1.5 Originality of the Research Works

The originality of this research work involved the effective growth control using applied current density and precursor concentration during EFAS method that allowed the effective tuning of the size, morphology and tip shape of the 1-D ZnO nanostructures (nanorods, nanocones and nanoneedles) and this discovery is original and novel. The effects of current density and precursor concentration on the structural and optical properties of ZnO nanostructure arrays synthesized on PSi substrate were investigated and reported. The fabrication of fast response-recovery time of the MSM ultraviolet (UV) photodetectors based on the needle-shaped and cone-shaped ZnO nanostructure arrays on PSi substrates was studied and reported.

1.6 Outline of the thesis

Chapter 1 contains a brief introduction of the properties, synthesis approaches, and applications of ZnO nanostructures, main research problem and motivation, scope of study, objectives of the thesis, and originality of the research works.

Chapter 2 presents the theoretical background and literature review of the growth procedures, structural properties, optical and electrical features as well as applications of ZnO and ZnO nanostructures.

Chapter 3 provides the general principles of tools and techniques applied for the synthesis and characterizations of one-dimensional ZnO nanostructures. After that, the synthesis processing of one-dimensional ZnO nanostructures and fabrication

processing of UV photodetector devices based on the ZnO nanoneedle and nanocone arrays produced using EFAS technique are also discussed.

Chapter 4 presents the results related to the growth and characterizations of 1-D ZnO nanostructures grown on PSi substrates. Included are results on the effects of current density and precursor concentration on morphology, structural, and optical characteristics of ZnO nanostructure arrays.

Chapter 5 focuses on the fabrication of UV photodetectors using vertically-aligned ZnO nanoneedle and nanocone arrays synthesized on PSi substrates and their optoelectronic properties.

Finally, Chapter 6 offers the conclusions of this research and recommendations for future work.

CHAPTER 2

THEORETICAL BACKGROUND AND LITERATURE REVIEW

2.1 Introduction

In this chapter, the structural properties and optical features of ZnO materials are presented in order to achieve a general understanding of the nanomaterials utilized in this study. The literature review and a number of growth methods and preparation parameters of one-dimensional ZnO nanostructures by EFAS technique that influence the morphology and crystalline quality of the ZnO nanostructures are presented. Information on ultraviolet photodetector based on one-dimensional ZnO nanorod-like arrays and the basic theories of metal-semiconductor-metal photodetector as well as typical mechanism of photoconduction in one-dimensional ZnO nanostructures are addressed.

2.2 Nanomaterials

Nanomaterials and nanotechnology are expressions which have received huge publicity for the last two decades. In general, the nanotechnology word is used for the manipulation of individual objects into an atomic/molecular scale or for nanostructures created by lithographic technique, while nanomaterials are nano-scale particles which can be generated by chemical synthesis approaches and utilized in masses. In both cases, it is the considerable properties, different from those in the bulk phase, which caused the excitement. Nanomaterials are frequently considered to be an invention of modern science. Nanotechnology and nanoscience have developed at an enormous speed and have gained considerable popularity in recent years. Nanomaterials have been recognized in a wide range of modern usages because they offer unique attributes.

Nanostructured materials have drawn more interest from researchers due to their unusual mechanical, electrical and optical properties that are well-distinct from those of their bulk phases. Recent development in nanostructured materials have opened up new numerous applications in electronics, energy, materials chemistry, even biology, and catalysis. They contain a dimension of less than 100 nm (less than 200 nm in other classifications) and are classified conforming to their nano-scale dimensions [32]. Nanostructured materials include nanoparticles, quantum dots (0-dimensional), nanorods, nanowires, nanotubes (1-dimensional), thin films, nanosheets (2-dimensional), and nanospheres (3-dimensional).

Nanomaterials attract considerable interest due to their unique chemical and physical characteristics, which are very dependent on their nanostructure size and surface nature. These variations mostly from two main effects that are related to the nanostructure size. The first effect is the surface-to-volume effect, in which the high surface-to-volume ratio increases when the size of the particle decreases; clearly, the number of surface atoms increases with decrease in the particle size. Hence, the surface atoms bond less with the interior atoms of the partial surrounding, which alters the chemical and physical properties of the nanomaterials [32]. Thus, the unique properties of materials in the nanometer scale, such as having a dimension size of greater than 10 nm but less than 200 nm, are induced solely through effects of high surface-to-volume ratio. The second function is the quantum confinement effect, which occurs once the size of the particle approaches the material exciton Bohr-radius, where the electronic and optical properties of nanostructured material will significantly alter from the bulk nature [33]. Several kinds of synthetic techniques have been used to generate the nanostructured materials. These methods include the gas phase methods, liquid phase techniques, and mixed phase syntheses. The choice of suitable method is important to

achieve the success or failure of the produced nanostructured materials, because chemical and physical properties and applications of the nanomaterials are strongly dependent on how they are synthesized. For recent decades, the importance of choosing a suitable approach in forming the materials of nano-scale has been a motivating force for the expansion of new methodologies [34].

2.3 Overview of ZnO and ZnO nanostructures

ZnO a II–VI compound semiconductor is one of the most outstanding semiconductors in the metal oxide family, an inherently n-type semiconductor, and transparent conducting oxide-semiconductor material. ZnO nanostructures have attracted more attention of researchers for the reason that they have important properties such as direct vast band gap of (3.37 eV) which is useful for photonic applications, a great optical gain which is larger than that of GaN [35], and a high-exciton binding energy of (60 meV) which is larger than that of ZnSe (22 meV) and GaN (25 meV) [36]. Due to these properties, ZnO nanostructure is a more promising material in excitonic emissions as well as lasing applications even at room temperature compared by other materials. ZnO is a versatile efficient material that have been generated via variety chemical and physical fabrication techniques in numerous group of growth morphologies, including single crystals, powders, thin films, and nanostructures [37], for instance nanotetrapods, nanoparticles, nanowires, nanofibers, nanorods, nanotubes, nanocombs, nanosheets, nanonails, nanoflowers, and nanobelts. These unique ZnO nanostructured material have received great attention owing to their much potential for a numerous of applications, especially their distinguished performance in photonics, and optics electronic. These novel nanostructural ZnO materials reveal two great properties, namely, the quantum confinement effects, high

surface to volume ratio, which are not observed in its bulk nature [38]. The unique nano-structural properties have created wide range of applications of ZnO nano-materials such as solar cells, UV detectors, chemical sensors, UV light emitting and piezoelectric devices.

2.3.1 Lattice parameters and crystal structures of ZnO

Most of the group II–VI compound semiconductors crystallize into either cubic zincblende or hexagonal wurtzite structure where each cation is encircled by four anions at the corners of a tetrahedron, and vice-versa. ZnO is a promising semiconductor material of the group-II element ${}_{30}\text{Zn}$ with the electronic configuration $(1s)^2(2s)^2(2p)^6(3s)^2(3p)^6(3d)^{10}(4s)^2$ and the group-VI element ${}_{8}\text{O}$ with the electronic configuration $(1s)^2(2s)^2(2p)^4$.

The crystal structures shared by zinc are three forms: rock-salt structure, cubic zinc-blende structure and hexagonal wurtzite structure. The rock-salt (NaCl), and cubic zinc-blende structures, are indicated in Figure 2.1 [39]. The rock-salt type structure is a high pressure metastable phase, which occurs at approximately 10 GPa [40], whilst zinc-blende ZnO is metastable structure, which appears when ZnO is grown on cubic structures such as ZnS [41-43].

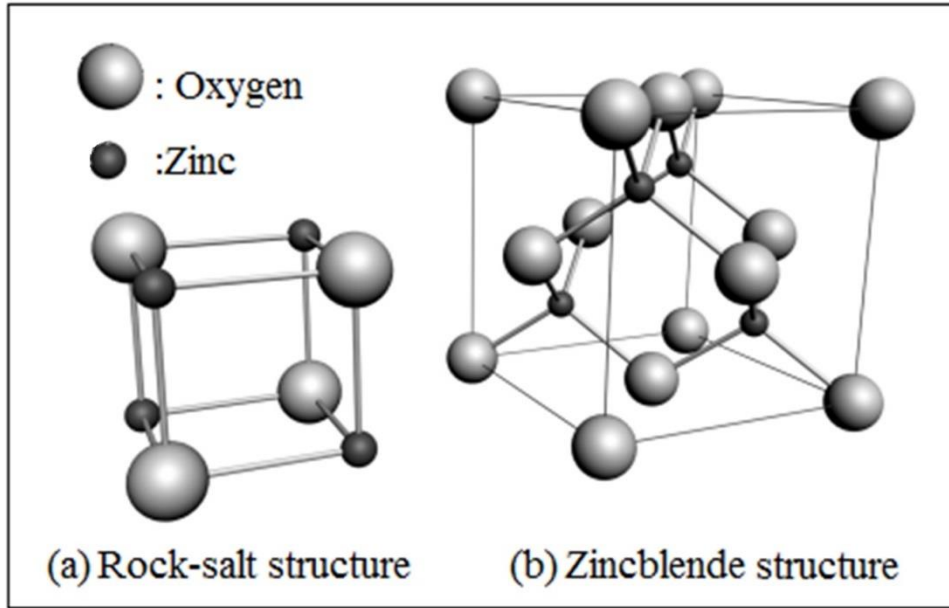


Figure 2.1: (a) The rock-salt and (b) zinc-blende structures of ZnO [39].

The crystal structure of the hexagonal wurtzite is zinc atoms encircled by four oxygen atoms at the corner of a tetrahedron and vice-versa [32]. Under ambient temperature and pressure, zinc oxide crystallizes in the hexagonal wurtzite type structure as well as its phase is thermodynamically stable, as schematically shown in Figure 2.2 (a). Hexagonal wurtzite structure is the most stable structure of ZnO; it contains of multiplanes of tetrahedral coordinates of O^{2-} with Zn^{2+} ions stacked alternatively along the c-direction, as shown in Figure 2.2 (a) [39]. The wurtzite structure contains an unit cell of hexagonal with lattice parameters, a and b lay in the x - y plane (which consist an angle of 120° and have equal length), and c lattice parameter is parallel to the z -axis, as demonstrated in Figure 2.2 (b) [39]. Figure 2.3 represents several lattice planes and direction with their Miller-indices in a hexagonal unit cell [44]. The values of lattice parameters of the hexagonal unit cell at room temperature are $a = b \approx 3.2495 \text{ \AA}$ and $c = 5.2069 \text{ \AA}$. In an ideal wurtzite crystal of ZnO structure has the axial ratio of $c/a = (8/3)^{1/2} = 1.633$, which changes in response to strain/stress [45]. Experimentally, for structure of hexagonal wurtzite of ZnO, the real

value of c/a was specified in the range $c/a=1.593-1.603$ [46]. Due to the lack of center symmetry of the wurtzite structure, ZnO reveals piezoelectric properties that arise from atomic scale polarizations (owing to the relative movement of the anions and cations in the crystal). In the tetrahedral structure, the zinc atom is bonded with four oxygen atoms, forming ionic dipoles with zero net charge. Therefore, the mass center for negative and positive atoms coincides. When the force is exerted along the c axis, the center of mass will no longer coincide, which produces the piezoelectric phenomena.

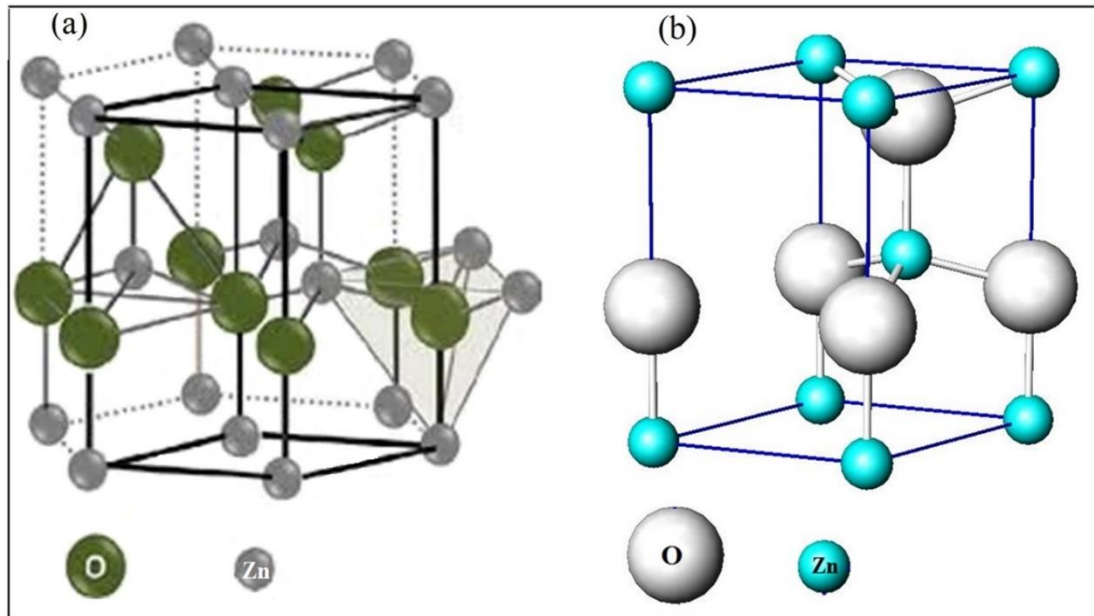


Figure 2.2: (a) The hexagonal wurtzite structure and (b) hexagonal unit cell of ZnO [39].

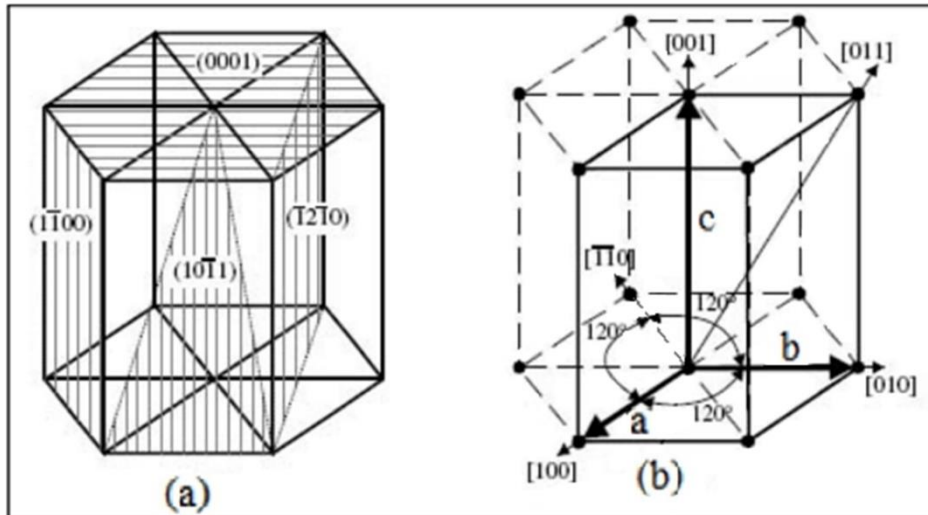


Figure 2.3: (a) Miller indices of several lattice planes in a hexagonal lattice of ZnO and (b) hexagonal unit cell and indices of several lattice directions [44].

2.3.2 Optical properties of ZnO

ZnO nanostructure is a well-known wide bandgap semiconductor with a bandgap of (3.37eV). It has a large absorption coefficient at near band edge, high excitonic binding energy of (60 meV) at room temperature, and efficient radiative recombination. Based on these fascinating properties, this nanostructure can be a promising material for using as photonic and sensing applications. Optical transitions in nanostructure mainly have been studied using photoluminescence spectra at room temperature. The photoluminescence spectra of ZnO normally consist of a sharp emission located at UV region (around 380 nm) and a visible broadband emission centered (ranging in 450-800 nm). The UV emission is attributed to the near-band-edge of free exciton recombination, while visible emission is probably originated from impurities and/or defects of ZnO, such as hydrogen interstitials, oxygen vacancies, and Zn interstitials, which produce sub-band levels inside the band-gap [47]. The UV peak intensity ratio to the defect-related peak intensity characterizes the ZnO materials quality.

Displacements in the situation of the PL peak of ZnO nanostructures in different sizes have been appeared in the PL spectra. One possible reason for the blue shift in the UV emission of ZnO nanostructures with size decrement is the quantum confinement effects [48]. Various native defect concentrations have also been proposed as a reason for the alterations in the position of the UV emission in numerous ZnO nanostructures with comparatively large dimensions. The defects density on the surface is greater than in the bulk [49], therefore displacements in the position of the PL spectra because of the various concentrations of defects are expected to appeared in nanostructures with different sizes due to various surface area to volume ratios. Thus, the PL spectrum shape as well as the position of the UV emission can be arised by the density of defects in nanostructures.

Even though there have been numerous reports of the PL spectra relate ZnO nanostructures with weak visible (defect) emission and strong UV emission [1], in some instances the UV emission peak is shorter than the visible emission peak [50] or solely visible emission peak [51]. When the PL measurements of diverse ZnO nanostructures were conducted under similar excitation conditions, the UV peak intensity ratio to the defect-related peak intensity can characterize the crystalline quality of ZnO nanostructures materials. Several various peaks in the visible spectral region (the range of from 405 nm to 640 nm) have been appeared in the PL spectra of ZnO nanostructure, which is attributed to the emission of defect [52]. The deep-level emissions (DLE) in the range of visible are owing to the recombination of photo-generated holes with singly ionized charge states in the intrinsic defects, such as oxygen vacancies, impurities, and Zn interstitials [53]. Oxygen vacancies occur in three multiple charge states: neutral oxygen vacancies, doubly ionized, and singly ionized [54]. Zainizan et al. [55] described indigo emission (the range of from 405 nm

to 440 nm) which is attributed to electron transition from the band of conduction to the oxygen interstitial, which is the defect of acceptor in intrinsic ZnO. The blue emissions ranging from 440 nm to 490 nm was produced from the electron transitions from the shallow donors level of the zinc interstitials and the oxygen vacancy to the valence-band [56]. The green emission ranging from 490 nm to 560 nm is the most usually appeared defect emission in ZnO nanostructure materials, which is attributed to the defects of singly ionized (oxygen vacancy). The yellow and orange emissions ranging from 560 nm to 630 nm were produced from the electron transitions between the energy levels of interstitial zinc and oxygen. Eventually, the red emission (the range of from 630 nm to 700 nm) is attributed to the emissions combination ascribed to the doubly ionized (oxygen vacancy) and interstitial oxygen [57].

Moreover, the luminescence properties of materials likewise provide information onto the radiative recombination that happens within a band gap. Therefore, the recombination of an electron (e^-)–hole (h^+) pair that generates light is known as radiative recombination, and those that do not generate light are called as non-radiative recombination. The radiative recombination produces photons with the energy corresponding to their transitions inside the band-gap. The non-radiative recombination emit the vibrations energy to the lattice in the form of phonons.

2.4 Overview of substrate

Up to now, large-scale arrays of ZnO nanostructures have been successfully synthesized onto various substrate types by different approaches. The surface morphology and structural type of the substrates and their lattice mismatch with a special nanostructure are significant parameters, which control the morphology and nature of the produced ZnO nanostructures.

2.4.1 Porous silicon (PSi) substrate

Porous nano-structure is one of the known nanostructured materials. The porous of description implies that billions of nano-sized holes are performed inside the materials. The ratio of the amount of a fraction of the volume of voids over the total volume is called the porosity. This term is used in various fields, including ceramics, metallurgy, pharmaceuticals, materials, manufacturing, construction, and earth sciences [58]. A common porous material is the porous semiconductor, which has promising for optoelectronic usages. Especially, broadening in band gap, tunable physical properties, and large surface-to-volume area are some of its properties that can be applied for the expansion of novel sensing devices [59]. The Porous semiconductor has been extensively studied in the past decades due to its adjustable roughness, low cost, and its special optical properties for instance band-gap shift, enhanced luminescence intensity, and improved photoresponse [60].

Among porous semiconductor materials, porous silicon (PSi) is an intensively studied material due to its adjustable roughness, large internal surface, high resistivity, low cost, and strong surface absorbability. When used as a template, nano-porous materials can be used as substrates to grow ZnO nanostructures [61, 62]. PSi has opened new possibilities for the silicon-based integrated circuits owing to its remarkable electronic and optical properties. Applications of PSi include highly efficient electroluminescent devices, photo detectors, surface acoustic wave devices, and devices that exhibit visible photoluminescence at room temperature, have been previously studied [63-66]. The PSi layer is a suitable material for accommodating the deposition of ZnO film on the porous surfaces that possess a large internal surface area, strong absorbability, and high resistance [67]. The integration of ZnO film and a PSi

layer is significant because the deposition of high quality ZnO film on a PSi layer can reduce thermal expansion stress and a large mismatch of lattice constants [68]. The PSi is quickly becoming a versatile electronic and increasingly important material in today's production technology. Its reactive porous nature allows for the selective formation of unique electronic components and mechanical nanostructures. PSi is an entrant for silicon based optoelectronic applications, such as solar cells, light-emitting and sensing devices [69, 70]. PSi nanostructures can be fabricated on silicon wafer by using photo electrochemical etching of silicon in hydrofluoric acid based material. PSi has been widely studied amongst porous semiconductor materials owing to PSi has strong surface absorbability, large internal surface area, high resistivity, and applications in developing optoelectronic devices [71]. PSi layers can reduce large mismatches in thermal expansion coefficients, and lattice constants, therefore reducing the large stress between silicon substrates and ZnO nanostructures [72, 73]. The combination of PSi substrate and the ZnO nanostructures can be considered as a white light source generated from red emission from the PSi layers and with the green and the blue UV emissions from ZnO nanostructures [74]. The ZnO/PSi layers also reveal superior luminescence properties, which satisfy the electrical and optical requirements of display technologies. In addition, various kinds of nanomaterials especially ZnO nanostructures have been synthesized on PSi substrates by numerous method. For example, Eswar et al. [75] reported the growth of ZnO nanostructures on the seeded PSi via hydrothermal immersion technique. Prior to this process, a ZnO thin film was first deposited on the PSi substrate as seed layer by spin coating method. Rusli et al. [76] reported the formation of large area high density ZnO nanostructures on the PSi substrates at growth temperatures range (600-1000 °C) using a thermal evaporation method. Rajabi et al. [77] fabricated ZnO nanorods and tetrapods on PSi substrate with

and without an Au catalyst by the chemical vapour transport and condensation technique. Vasquez-A et al. [78] used the direct current sputtering to study the transport mechanisms in PSi layers and ZnO/PSi layers/c-Si heterostructures. Cai et al. [68] synthesized high quality oriented ZnO films on PSi substrates using radio frequency magnetron sputtering and sol-gel spin coating methods. Kou et al. [79] employed the electrodeposition technique to fabrication well aligned ZnO nano-flowers and nano-sheets on PSi at various applied potentials. In the present study, the needle-shaped and cone-shaped ZnO nanostructure arrays are synthesized on PSi substrates using a facile low temperature method. The optical and structural properties of high density ZnO nanostructures are characterized. These findings have great potential for applications in the MSM ultraviolet photodetector and the detection of different chemicals.

2.5 Overview of electric field-assisted aqueous solution technique

2.5.1 The electric field-assisted aqueous solution technique

Various substrate types are employed to synthesize 1-D ZnO nanostructures by different methods. Hsu et al. [73] reported the improvement of ZnO nanowire orientation on PSi using the vapor–liquid–solid process. Abdulgafour et al. [80] created a ZnO nanocoral reef on PSi substrate without any catalyst by the simple thermal evaporation technique. Rajabi et al. [77] prepared ZnO nanorods and tetrapods on PSi substrate with and without an Au catalyst through the chemical vapor transport and condensation approach. However, these methods use complicated procedures and expensive apparatuses due to high temperature processes. The EFAS method is a highly appropriate technique for the synthesis of 1-D ZnO nanostructure arrays because it is a simple, uses low temperature, scalable, and low cost.

Several methods have been employed to synthesis of ZnO nanostructures on various types of substrates and the synthesis can be classified as a solution-based technique and a vapor-based technique. Vapor-based method includes thermal evaporation, vapor–liquid–solid, chemical vapor deposition, metal organic chemical-vapor deposition, chemical vapor transport, molecular beam epitaxy, and condensation procedure. Vapor-based approaches can synthesis high-quality ZnO nanostructures under high-vacuum and well controlled conditions. However, these methods have several major disadvantages such as high cost of equipment, high temperature complexity, and are not suitable for growth of ZnO nanostructures on flexible polymeric substrates because of the high-growth temperature [54]. Solution-based method includes hydrothermal technique, solvothermal technique, chemical bath deposition, and electric field-assisted aqueous solution technique. The solution-based procedure has been used greatly for mass production of oxide nanomaterials, semiconductors, and metals with good controls of the composition and morphology – the advantages are its low-growth temperature, simplicity, significant potential to large-scale production, lower cost, and environmentally friendly processing. The process is called solvothermal when an organic or inorganic (non aqueous) solvent is used to dissolve the materials (other salt/nitrite solution) and the complete materials under high pressure as well as high temperature. When water is utilized as the solvent of the starting materials inside a closed vessel at high-pressure (range of 10^6 Pa to 10^8 Pa) and high-temperature (range of 100 °C to 1000 °C), the technique is called hydrothermal [81]. As for chemical bath deposition, water is applied as a solvent to form the materials under ambient pressure and low temperature (lower than 100 °C) [82].

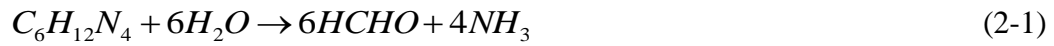
The electric field-assisted aqueous solution process is similar to electrochemical deposition except that the temperature can be selected higher than 90 °C while the electrochemical deposition is typically conducted at a considerably lower temperature (usually from 60 °C to 90 °C). Accordingly, the process can be called EFAS when water is employed as a solvent of the material under the temperature around 100 °C and ambient pressure. The optical properties of nanostructured materials can be further improved if growth occurs at a higher temperature. Thus, the EFAS method has potential to the decrease of defect density of deposited nanostructures. The EFAS is a very powerful procedure to achieve good uniformity, high purity, and large area fabrication of ZnO nanostructures, because it applies a strong-external driving force to create the reactions. The synthesis of ZnO nanostructures can be implemented on a general sample, curved or flat, with or free the seed-layer. Moreover, under apply such an external electric-field, well-alignment nanostructure arrays and stronger interfacial adhesion to the sample have been produced [83, 84]. The EFAS process can be performed in an aqueous electrolyte solution using a simple two electrode home-made Teflon cell. The sample is placed on the external wall of Teflon cell and a platinum wire is applied as the counter electrode (anode) as well as the sample is employed as the working electrode (cathode). The schematic illustration of the experimental set-up is shown in Figure 3.2.

To date, EFAS technique can synthesize various nanostructured semiconductor materials with good electrical and optical properties, and high crystallinity in different morphologies such as nanocrystalline thin films, nanosheets, nanoneedles, nanotubes, nanorods, nanowires, and nanoflowers. The structural, morphology, and optical properties of these nanostructures, as well as the thickness of deposited film can be

readily controlled through varying growth parameters, including current density, precursor type, growth time, temperature of growth, and solution concentration.

2.5.2 Mechanism of electric field-assisted aqueous solution technique

The mechanism of EFAS technique for growing of ZnO nanostructures can be described as follows. In this procedure, the substrate and the platinum electrode are positioned in an electrochemical cell containing the aqueous solution of zinc nitrate hexahydrate ($Zn(NO_3)_2 \cdot 6H_2O$) and hexamethylenetetramine ($C_6H_{12}N_4$) that act as the source of Zn^{2+} and OH^- ions, respectively. In the EFAS method, the growth of the ZnO nanostructures usually occurs based on the production of hydroxide OH^- ions under the current density. The Zn^{2+} ions react with OH^- ions thereby forming zinc hydroxide $Zn(OH)_2$. ZnO is created out on the sample via a dehydration reaction of ($Zn(OH)_2$). The formation of OH^- ions is generally affected by the current density. The reactions involved in the solution can be described by the following formulae [85]:



2.5.3 Numerous advantages of use the electric field-assisted aqueous solution technique

The synthesis of nanomaterials requires an atomistic deposition process and extreme control over the deposition. Electrochemical strategies offer important advantages and unique possibilities in the development of nanomaterials and nanostructures. EFAS technique as an atomic deposition process can be used to synthesize nanomaterials. EFAS is a unique procedure in which a variety of materials can be processed including metals, ceramics and polymers. The obvious advantages of this method are as follows:

- a. Rapidity and high purity.
- b. Low cost and free from porosity.
- c. Industrial application.
- d. Produce coatings on widely different substrates.
- e. Higher deposition rates.
- f. Ability to create structural features with the sizes ranging from nm to μm .
- g. Ability to generate compositions unattainable using other methods.
- h. The possibility of creating of simple low-cost multilayers in different systems.

2.6 Overview of one-dimensional ZnO nanorod-like arrays growth conditions

2.6.1 Mechanism of one-dimensional ZnO nanorod-like arrays growth conditions

Aligned one-dimensional ZnO nanorod-like arrays can play an important role in a broad range of applications in the electronic and optoelectronic devices. The structural, optical and electrical properties of the ZnO nanorod-like arrays strongly depend on their morphology and shape. Consequently, whole understanding of the influence of growth parameters concerning growth mechanism, morphology, and size of the one-dimensional (1-D) ZnO nanostructures are essential. The mechanism for the effects of precursor concentration and growth time of 1-D ZnO nanorod-like arrays can be explained based on the chemical reactions in the EFAS process as well as theory of nucleation and formation of ZnO nanocrystal. In the chemical process of 1-D ZnO nanorod-like arrays growth, $C_6H_{12}N_4$, water molecules and $Zn(NO_3)_2 \cdot 6H_2O$ in the solution provide OH^- , O^{2-} and Zn^{2+} ions, respectively. The reactions of chemical related to the growth process of 1-D ZnO nanorod-like arrays in the EFAS technique (mentioned in prior section, i.e. Eq. 2.1 to Eq. 2.5) can be effectively controlled via changing the reaction parameters comprising precursor concentration, current density, growth time, and growth temperature. Wurtzite structure of 1-D ZnO nanorod-like arrays has two kinds of crystal planes consisting polar (0 0 1) surface, and nonpolar surfaces such as (1 0 1) and (1 0 0). The crystal planes have faster growth rate due to their higher surface energy, consequently, the growth rate of the surfaces in the [0 0 1] direction can be more than that of the surfaces in the [1 0 0] direction [86]. The aspect ratio of the as grown 1-D ZnO nanorod-like arrays can also be specified through the relative growth rate of the polar surface and the surface of non-polar [87].

Therefore, while the precursor concentration is increased, the amount of $Zn(OH)_2$ that is produced from the precursor solution will be increased, and as a result whereby an increase in the growth rate of 1-D ZnO nanorod-like arrays during EFAS synthesis [88]. The endothermic nature of these processes prevent the growth

of 1-D ZnO nanorod-like arrays in the $[0\ 0\ 1]$ directions. Consequently, thicker and shorter nanorod-like arrays can be fabricated under greater precursor concentration. The dependence of the deposition time on the chemical solution employed in the reaction is one of the other important parameter, which reveals the thermodynamics and/or kinetics processes owing to its close relation to the concentration change and reaction rate in the reaction process. With the increase of electrochemical deposition duration, diameter and length of the nanorod-like arrays will be increase. When the reaction time is persisted to appropriate time, then the diameter of the 1-D ZnO nanostructures does not get increase obviously, while their length is increased. The non-polar $(1\ 0\ 1)$ plane of ZnO crystal structure has lower surface energy and also greater stability compared with the polar $(0\ 0\ 1)$ plane. Hence, the ZnO nanostructures grow mainly along the greater surface energy $(0\ 0\ 1)$ direction. Furthermore, the diameter of the nanorod-like arrays does not clearly increase, because the density of the ZnO nanorods is higher and the horizontal space is smaller [89].

2.6.2 Literature review of one-dimensional ZnO nanorod-like arrays

Ko et al. [88] synthesized ZnO nanorod arrays on a flexible substrate via the electrochemical deposition process and investigated the surface morphology and optical properties of ZnO nanostructures using changing the applied cathodic voltages. They found that with the increase of voltage, the growth rate is increased. In other words, the average width and length, density and vertical alignment of ZnO nanorod-like arrays increased with increasing applied voltage from 1.6 V to 2.4 V. Amin et al. [90] investigated the influence of precursor concentration and growth time on the morphologies of ZnO nanostructures synthesized on Si substrate using hydrothermally approach. They found that the fabricated ZnO nanostructures at precursor